SCIENTIFIC REPORTS

OPEN

SUBJECT AREAS:
SEISMOLOGY
PETROLOGY
VOLCANOLOGY
GEOCHEMISTRY

Received
20 May 2014

Accepted
22 July 2014

Published
9 September 2014

Correspondence and requests for materials should be addressed to L.P. (lucia.pappalardo@ingv.it)

Petrological and seismic precursors of the paroxysmal phase of the last Vesuvius eruption on March 1944

Lucia Pappalardo[1], Luca D'Auria[1], Andrea Cavallo[2] & Stefano Fiore[1]

[1]Istituto Nazionale di Geofisica e Vulcanologia, Sezione di Napoli Osservatorio Vesuviano, Via Diocleziano 328, I-80124 Napoli, Italy, [2]Istituto Nazionale di Geofisica e Vulcanologia, Via di Vigna Murata 605, 00143 Roma, Italy.

Abrupt transitions in style and intensity are common during volcanic eruptions, with an immediate impact on the surrounding territory and its population. Defining the factors trigger such sudden shifts in the eruptive behavior as well as developing methods to predict such changes during volcanic crises are crucial goals in volcanology. In our research, the combined investigation of both petrological and seismic indicators has been applied for the first time to a Vesuvius eruption, that of March 1944 that caused the present dormant state of the volcano. Our results contribute to elucidate the evolution of the conduit dynamics that generated a drastic increase in the Volcanic Explosivity Index, associated to the ejection of huge amount of volcanic ash. Remarkably, our study shows that the main paroxysm was announced by robust changes in petrology consistent with seismology, thus suggesting that the development of monitoring methods to assess the nature of ejected juvenile material combined with conventional geophysical techniques can represent a powerful tool for forecasting the evolution of an eruption towards violent behavior. This in turn is a major goal in volcanology because this evidence can help decision-makers to implement an efficient safety strategy during the emergency (scale and pace of evacuation).

Sudden transitions on eruptive style and intensity are frequently observed during volcanic eruptions with an immediate impact on the surrounding territory and its population. A recent severe example is the eruption of the Mount Sinabung in Indonesia, started on September 2013 and culminated on February 2014 with the death of at least 14 people as a result of the rapid increase of explosive behavior, which occurred just after residents, that lived more than five kilometers from the mountain, had been allowed to return home following a temporary decline of volcanic activity[1].

This behavior is also known to occur in mafic volcanoes[2]. The Stromboli volcano (Tyrrhenian Sea), known for its persistent moderate activity, has undergone in the last decades sudden vulcanian explosions, abruptly interrupting effusive eruptions[3,4]. Such events have been attributed to the rapid ascent of gas-rich batches of magma, similar in composition to the ongoing lava flows[5–7].

The trigger for such sudden shifts in the eruptive regime has been generally attributed to various reasons (such as magma chamber and/or conduit processes; vent geometry; magma/water interaction etc.), however it remains poorly understood for many eruptions and hence, difficult to predict. Fundamental information on subsurface magma behavior and its influence on eruptive style can be obtained by the compositional and textural studies on volcanic rocks. These studies, applied to the rocks emitted during recent well-monitored eruptions, have revealed crucial relationships between the petrography of emitted rocks and the pre-/syn-eruptive geophysical signals[8–10].

However, most studies have focused on intermediate to felsic magma eruptions, while mafic magmas remain less explored. The last mafic magma eruption of Vesuvius occurred on March 1944, consisting of an initial effusive phase (supplementary table 1) culminated in a paroxysmal explosive activity, provides an unusual, and unique for Vesuvius, opportunity to investigate this key issue. The eruption in fact, lasted about 10 days, was well documented both for volcanological and seismological record, due to the detailed work of Giuseppe Imbò[11] that was then director of the Vesuvius Observatory. Recent studies have shown that the intensity of this eruption and its effects on territory and population have long been underestimated, perhaps due to the Second World War going on[12]. After an initial effusive phase I (18–21 March), during which two towns in the west of the volcano were partly destroyed by the passage of lava flows, followed by a phase II characterized by the succession of eight lava fountains (21–22 March), the eruption culminated quickly in a violent explosive phase III (22 to 23 March) in which the eruption column exceeded 10 km altitude on the crater and ash carried by winds reached considerable

distances from Vesuvius, up to Albania and Yugoslavia[13]. This paroxysmal phase lasted only 24 hours, since later the explosions became discontinuous and the ash cloud reached altitudes not exceeding 2 km from the crater (23–29 March - phase IV). The examination of new accounts of witnesses has shown that probably the number of victims (both humans and animals) associated to this paroxysmal phase may be greater than previously considered, due to the dispersion of the volcanic ash over wide areas[14]. Moreover, the mafic (phonotephrite-tephrite) character of the volcanic products makes more difficult the identification of the reasons that led to this sudden and drastic increase in the Volcanic Explosivity Index (VEI) that generally is instead associated with the emission of sialic magmas. We have conducted a detailed geochemical and textural study on the full succession of erupted products and compared the obtained results with the geophysical data recorded throughout the course of the eruption by Giuseppe Imbò.

The obtained results contribute to shed light on the evolution of conduit dynamics that triggered a sudden increase in the VEI, associated to the emission of a large amount of volcanic ash, that covered wide areas with a strong impact on territory and population.

Moreover our results suggest that the main phase of the volcanic paroxysms can be preceded by important changes in petrological indicators, correlated to geophysical signals that if monitored during volcanic crisis could provide fundamental clues about the ongoing eruption dynamics. This was also observed during recent well-monitored eruptions (e.g. the 2011–2012 El Hierro, Canary Islands, submarine eruption), for which the time correlation between magma evolution and the monitored geophysical signals has been evidenced and used to track the geological processes accompanying the magma movement towards the surface[15].

Results

Petrological indicators. All the analyzed rocks are porphyritic characterized by euhedral phenocrysts (crystals $>$ 0,1 mm) included in a groundmass consisting of microlite ($<$ 100 micron) crystal population and tephritic to phono-tephritic glass (supplementary Table 2).

Phenocrysts comprise plagioclase, clinopyroxene, olivine and leucite as prevalent phases, while titanomagnetite and biotite are subordinate. Apatite is a common accessory crystal. Groundmass glass is composed prevalently of feldspar, clinopyroxene, leucite and magnetite microlites.

In general, none important difference has been observed in the composition of phenocrysts from rocks emitted during the different phases of the eruption (supplementary Table 3). This suggests that their crystallization occurred under similar chemical-physical conditions. Particularly, plagioclase crystals have composition ranging from bytownite (An_{85}-Ab_{12}) to labradorite (An_{62}-Ab_{34}), while pyroxene compositions fall in the diopside field and show a general trend toward Fe-rich composition (En_{39-36}-Fs_{11-14}). The olivine (Fo_{71-90} Fa_{10-30}) and leucite crystals show moderately homogeneous composition (supplementary figure S1).

In spite of the uniform composition of phenocrysts and groundmass glass, the analyzed volcanic samples show different textural characteristics in microlites, depending upon which stage of the eruption they represent. Thus suggesting that the variations in the conditions of magma ascent and degassing during the growth of microlites in volcanic conduit could be the main cause of the observed changes in the eruptive style during the course of the eruption.

In particular, lava (effusive phase I) and subordinately scoria (lava-fountains phase II) samples are characterized by larger prismatic plagioclase (60–80 micron) associated to smaller blocky clinopyroxene (30 micron). While pumice and ash (sustained-column III phase and vulcanian - IV phase), contain sparse smaller acicular clinopyroxene and in minor amount plagioclase (15-10 micron) (figure 1, table 1). Moreover, number density (number of microlites per unit area) shows the lowest values in lavas (11673) and scorias (10895-25803) while they increase in pumices and ashes from the phase III (40000) and phase IV (35000) (table 1).

Following the pioneering work of Marsh[16,17] and Cashman and Marsh[18], the size of microlites and their abundance can be represented in a semi-logarithmic plot of crystal size distributions (CSD). Generally, CSDs show a linear trend on log–linear plots, in a steady-state crystallization regime[16,17]. Kinking or curvature in the plot profile has been attributed to a complex crystallization history[19] (e.g. crystal accumulation and removal[17]; mixing of crystal populations[19–21]; compaction[22],).

For all the studied samples, larger-size plagioclase and smaller-size clinopyroxene microlites display straight CSD trends (figure 1 and table 1). Particularly larger plagioclase, that characterize prevalently lava and subordinately scoria groundmass, show gentle slopes (-30) and low intercept values (from -11 to -12), while pumice and ash commonly include smaller clinopyroxene and subordinately plagioclase microlites, with steep slopes (-175 to - 608) and a higher y-axis intercept (from -7 to -9) (figure 1).

Seismological indicators. Vesuvius Observatory is among the first institutions performing monitoring of an active volcano using seismological instruments[23]. In March 1944 two seismometers were operating at Vesuvius Observatory (V.O.): Vicentini (three component) and Omori-Alfani-Malladra (hereinafter O.A.M.) vertical component seismometer. Another three-component Wiechert seismometer was deployed at the "Istituto di Fisica Terrestre" (I.F.T.) of the University of Naples. In the following we compare the recordings of the O.A.M. and of the Wiechert, following the work of Imbò[24] (see Supplementary information Quadro IV and Quadro X).

Seismic signals, related to the 1944 eruption, are generally characterized by a background volcanic tremor, sometimes showing highly variable amplitudes. Different transients, emerging from the tremor, can be recognized[24]. They can be linked to both local earthquakes and volcanic explosions. The visual inspection of paper recordings of the 1944 eruption (supplementary figure S2), does not allow an unambiguous discrimination between these two typologies.

Imbò conducted a detailed analysis of these recordings, summarizing the observations in terms of various indices. He indicated aM as the maximum amplitude of the seismic trace within a given time window and aP as the "prevalent" amplitude of the background tremor within the same window. He performed this analysis over all the available paper recordings of the eruption. We consider here only the data from O.A.M. and the Wiechert seismometers, since they operated almost continuously during the considered interval, providing the most reliable data. The recordings of the Vicentini seismometer, as reported by Imbò[24], were often saturated during intervals of more energetic eruptive activity, do not allowing a quantitative estimation of the amplitudes.

In figure 2 we represent both the prevalent and the maximum amplitudes for the O.A.M. seismometer recordings from seismometer from March 21st to 23rd 1944. During the phase I they show a fairly constant value. During the phase II they show marked increments in correspondence of lava fountains[24]. During the transition between phases II and III, the amplitudes remain on high values, until they drop at the end of the first interval of the phase III at 17 : 53. This reflect a waning of the eruptive activity which lasts until 20 : 53 when it increases again, marking the beginning of the second interval (figure 2). This pattern is consistent for both the aM and the aP indices.

On the other hand, the amplitude ratio between the O.A.M. seismometer at V.O. and the Wiechert seismometer at Naples shows a different behavior. Values are fairly constant during the first and the second phase, showing a progressive drop at the beginning of the 8th

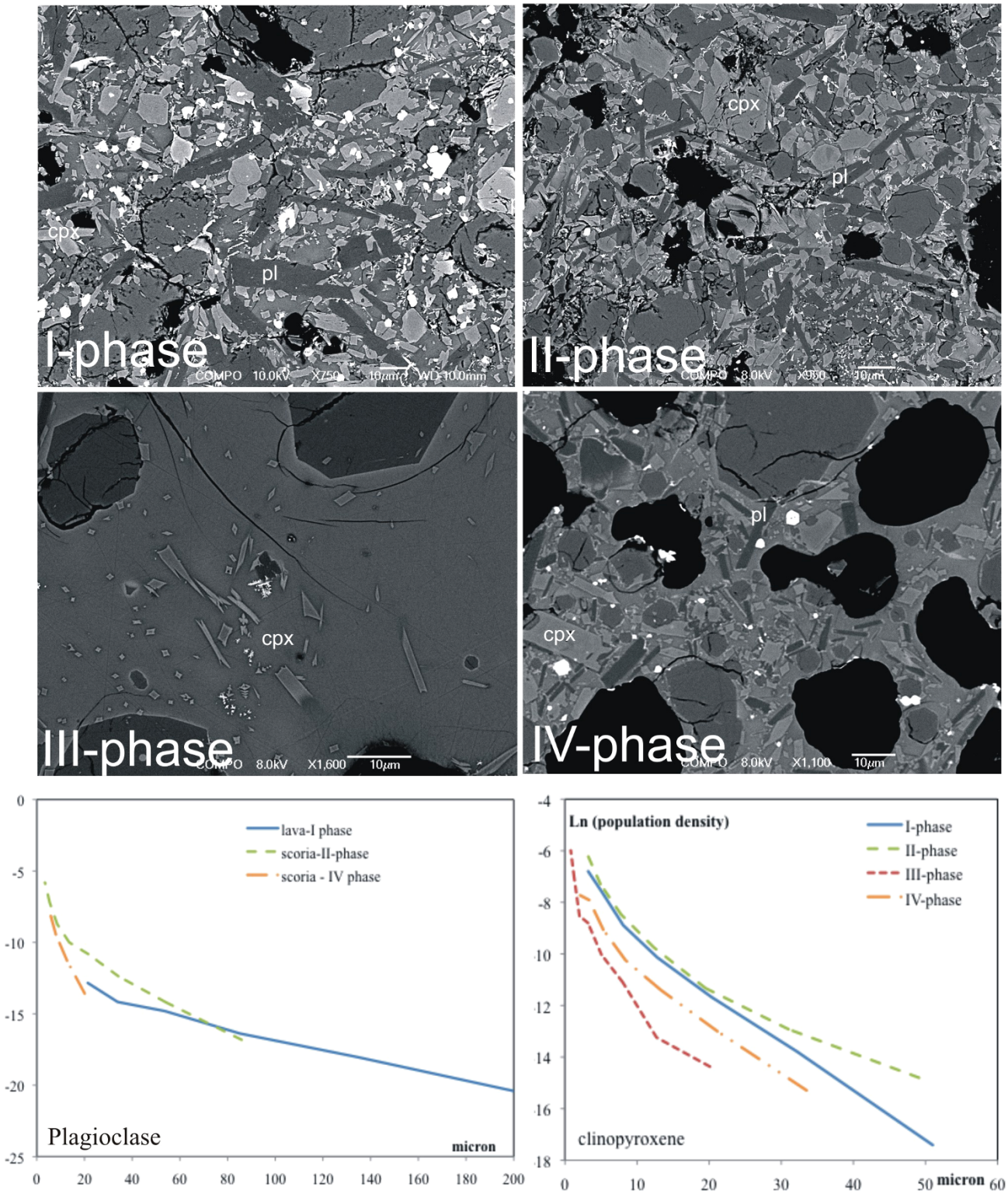

Figure 1 | Back-scattered electron (BSE) images of groundmass textural features in samples from the different stages of the Vesuvius 1944 eruption. Lava (phase I) and subordinately scoria (phase II) samples are highly microcrystalline with larger prismatic plagioclase associated to smaller blocky clinopyroxene. Pumice and ash (phases III and IV) contain sparse smaller acicular clinopyroxene and in minor amount plagioclase. Crystal size distribution plots display gentle slopes and low intercept values for larger-size plagioclase and higher y-axis intercept and steep slopes for smaller-size clinopyroxene.

lava fountain (figure 3). The decrease is more evident considering the ratio between the vertical component at O.A.M. (Zv) and that of the Wiechert (Zn), but it is also recognizable on the ratio between Zv and the horizontal component of the Wiechert (Hn) (figure 3).

The amplitude at O.A.M. remains high until the end of the first interval (figure 2), hence the decrease of the ratios is related to an increase of the amplitude at the Wiechert. During the second phase the amplitude at O.A.M. is tightly correlated to the lava fountain

Table 1 | Textural variations of microlites in samples from the different phases of the eruption

eruptive phase	sample	mag.	ncpx	npl	ntot	habit		Lmax		Total ref.area(μ2)	Na(mm²)	plagioclase		clinopyroxene	
						cpx	pl	cpx	pl			slope	intercept	slope	intercept
lava flow - I phase	LV44	300x	594	127	721	rectang prism	acicular	30	60	90519	-	−30	−12,13	−133	−7,3
lava flow - I phase	LV44	750x	174	65	239	rectang prism	rectang prism	30	60	20474	11673	−35	−12	−176	−7,67
lava fountains II- phase	SC1	600x	208	216	424	rectang prism	rectang prism	30	40	38916	10895	−120	−8,05	−175	−7,38
lava fountains II- phase	SC4	950x	270	82	352	acicular	rectang prism	30	40	13642	25803	−255	−7,69	−223	−6,05
lava fountains II- phase	SC9	800x	482	-	482	acicular	acicular	25	40	15000	32133	-	-	−203	−7
mixed explosions III-phase	T44B	550x	194	-	194	acicular	acicular	15	15	36247	-	-	-	−608	−9,38
mixed explosions III-phase	T44B	1100x	180	20	200	acicular	acicular	10	10	5000	40000	-	-	−429	−7
vulcanian IV-phase	T44T	500x	132	-	132	acicular	acicular	15	15	22349	-	-	-	−281	−8,54
vulcanian IV-phase	T44T	1100x	65	110	175	rectang prism	rectang prism	15	15	5000	35000	−402	−5,81	−305	−6,98

activity[24]. This has been observed, in modern times, also on other volcanoes like Kilauea[25] and Etna[26]. The seismic source relate to this kind of activity is generally very shallow (few hundred meters), making its amplitude to decay quickly at increasing distances from the eruptive vent. The V.O. is only 2 km apart from the Vesuvius crater, while the I.F.T. in Naples is about 14 km away from it.

Hence a likely explanation of the observed variation in the ratios is an increase in the activity of deeper seismic sources, which can be related to different phenomena occurring at greater depth. This hypothesis is supported by the observed variations in the amplitude ratios among different components at the Wiechert seismometer (figure 4). In particular we observe that, while the E/N ratio oscillates around 1 (with the higher variability during the phase II), the H/Z ratio shows a marked decrease since the beginning of the 8th lava fountain, following a trend very similar to the ratios shown in figure 3.

In conclusion, since the beginning of the 8th lava fountain, there is an increase in the activity of seismic sources, deeper than those related to the lava fountain activity, and possibly related to a different physical mechanism (e.g. earthquakes). These sources become progressively dominant during the first interval of the phase III.

Discussion

The homogeneous composition of phenocrysts and glass in all the studied rocks indicates that the magmas erupted in the different stages of the eruption, have crystallized at similar chemico-physical conditions. To determine temperature, pressure and water content during phenocrysts crystallization in the reservoir, we have used thermodynamic calculations based on the minimization of the free energy of Gibbs (MELTS Code[27,28], and PELE code[29]). In Melts calculations the following parameter ranges were assumed: pressure from 1000 to 4000 bar, QFM (quartz, fayalite, magnetite) oxygen fugacity ± 3 log units, and initial H_2O content from 1 to 6 wt %.

Among the calculated liquid lines of descent and mineral crystallization sequences produced by MELTS, those under conditions of water saturation, oxygen fugacity buffered along QFM-3, and pressures of ≥ 250–400 Mpa are in general agreement with the phenocrysts assemblage and modal abundance observed in the studied natural rocks (that was olivine ≤2% followed by clinopyroxene ≤20%, apatite ≤1% and magnetite ≤5% and later by plagioclase ≤20% and biotite≤5%[30],). Indeed, under lower pressure conditions (<250 Mpa), clinopyroxene always starts to crystallize earlier than olivine, that is present with higher modal abundance for the whole crystallization sequence in contrast to what observed in real rocks, (figure 5). The obtained results indicate that the crystallization occurred from a parental tephritic magma at near water-saturation condition, during cooling (T = 1150°C – 950°C) in a crustal reservoir located at depth between 16 and 10 km (P between 400 and 250 Mpa); the first precipitating phases are olivine and pyroxene, followed by magnetite, biotite and apatite and plagioclase. These results are in agreement with the pressure values obtained by using the volatiles (CO_2 and water) content measured on melt inclusions[31–33] trapped in olivine and diopside (figure 6), compared with the available solubility models. Moreover, in the explored pressure and temperature ranges, leucite never has appeared on the liquidus, this is also consistent with the volatile contents measured on melt inclusions in leucite that record CO_2 below detection limit and low H_2O content. This suggests the formation of this phase during a later crystallization event, at very low pressure (figure 6), probably during the ascent of the magma in volcanic conduit, also in agreement with experimental results indicating that the crystallization of leucite in Vesuvius magmas occurred at pressure <100 MPa[34].

Constraints on the magma ascent rate can be obtained by using the volatile content measured in groundmass glass (figure 6), whose composition corresponds to that of the residual liquid during degassing in the volcanic conduit. In particular, the low water content (H_2O

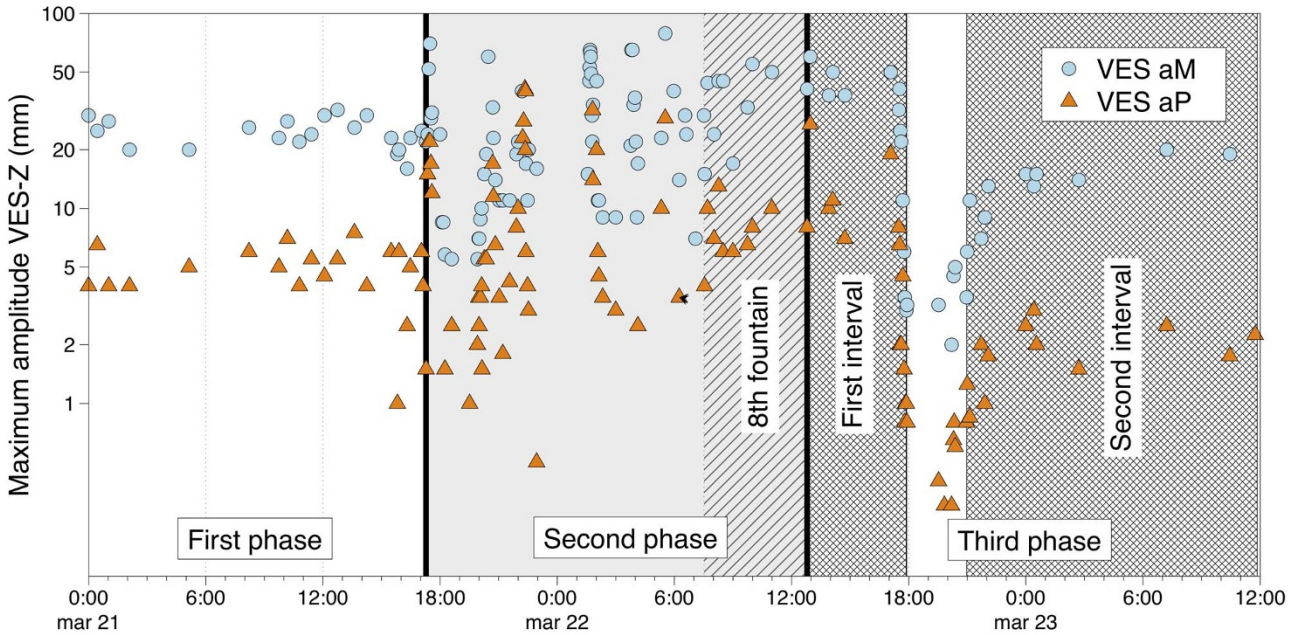

Figure 2 | Amplitudes at the O.A.M. seismometer from March 21st to 23rd 1944. aM means "maximum" amplitudes, while aP mean "prevalent". See text for details. Data from Imbò[24] The gray shaded area from 17 : 17 of 21st to 12 : 48 of 22nd indicates the duration of the eruptive phase II. The hatched pattern marks the interval of the last lava fountain of this phase. The crosshatched areas mark the first and the second intervals of the eruptive phase III.

wt% ~ 0.5), that characterizes the groundmass glass of lavas emitted at the beginning of the eruption, are compatible with a slow magma decompression, that favors the volatile exolution, bubbles coalescence (that controls magma permeability) and then removal of gas (including H_2O) from the liquid. On the contrary, the highest content of water (H_2O 1.5–3 wt%), in groundmass glass of scoria and ash of the explosive phases of the eruption, is indicative of a more rapid ascent, that prevents the removal of the gas phase, which then remains in contact with the liquid until the explosive fragmentation. Similar assumptions are suggested by Cl content behavior. Signorelli and Carroll[35] have shown that Cl content increases within the liquids saturated with both a H_2O vapor phase and a Cl-rich brine, as pressure decreases. The lavas of the phase I follow this Cl solubility model, corroborating the hypothesis of an initial slow ascending magma (figure 6b), while scoria and ash of the following phases show a constant Cl concentration, indicating a fast ascent which prevents fluid/melt Cl exchange.

This scenario is verified by the groundmass microlite textural variations detected in 1944 volcanic rocks, showing an evolution with time toward low values of crystallinity and mean microlite size, as well as a growth in crystal number density, associated to a progression in microlite shape that shifts from prismatic toward more skeletal (acicular, shallow-tail). Actually, decompression experiments[36–41] have revealed that groundmass microlite texture is strictly related to mechanisms and time of magma decompression in volcanic conduit. Particularly, under conditions of rapid ascent, due to high rate of undercooling (defined as the difference between the liquidus temperature and that of the magma) the crystallization is controlled by nucleation of new sites (nucleation-dominated regime); thus resulting in many tiny skeletal (e.g. hopper, shallow-tail, acicular shape) microlites. On the contrary in low ascending magma, growth of existing crystals prevails (growth-dominated regime) over nucleation due to the reduction over time of the degree of undercooling; thus resulting in fewer but larger (e.g. tabular, prismatic) microlites. Moreover, recent experiments[42] have determined that during higher-pressure decompression, crystallization occurs under growth-dominated regime; whereas at lower-pressure decompression crystal nucleation prevails. Therefore, we suggest that the largest prismatic plagioclase, that mainly characterize lavas emitted during the first phase of the eruption, have crystallized slowly under higher-pressure decompression conditions and can be associated to the magmatic intrusion during the widening of volcanic conduit; while the smaller acicular clinopyroxene observed prevalently in scoria and pumice from the subsequent explosive phases of the eruption are indicative of a fast decompression in the shallower part of the unlocked conduit.

Extimation of microlites crystallization time during decompression in the conduit can be obtained from the slope of the CSDs trends (if the crystal growth rate is known) using the following equation[16]: slope=-1/(G*T), where G is the growth rate and T is the crystallization time. Applying this equation to the CSDs trends of the different sized microlites observed in 1944 volcanic rocks, we have estimated the magma ascent rate at various depth in the conduit during eruption progression. Particularly, the largest plagioclases (characterized by gentle slope in CSDs) represent the earlier magma intrusion in the deeper conduit, while the smaller clinopyroxenes (steep slope in CSDs) reflect a later stage of ascent at shallower depth. Growth rate of groundmass plagioclase and clinopyroxene due to water exolution during magma ascent, are generally estimated to be between 10^{-7} to 10^{-8} mm/s[42–45] for mafic composition. By using the above range of crystal growth, we have calculated a minimum and maximum crystallization time for largest plagioclase (gentle CSD slopes) included in lavas, ranging from 38 to 4 days. Thus indicating the possible development of an ephemeral (in the order of months to days) shallow storage zone beneath the volcano, in which the earliest erupted magmas would have been arrested during the enlargement of the conduit. A volume of magma of 0.02 km^3 was erupted during the phase I, eventually stored for a short time in this shallow region. Imbò[24] reports a variation in the seismicity pattern since the beginning of March, about 20 days before the onset of the eruption, that corresponds to the intrusion of magma at shallow depth inferred on the basis of our petrological data. Moreover, microlite crystallization time calculated for the smaller clinopyroxene (steep CSD slopes) observed in the rocks emitted in the latter stages of the eruption, indicates that decompression became gradually faster, ranging from tens of hours at the begin-

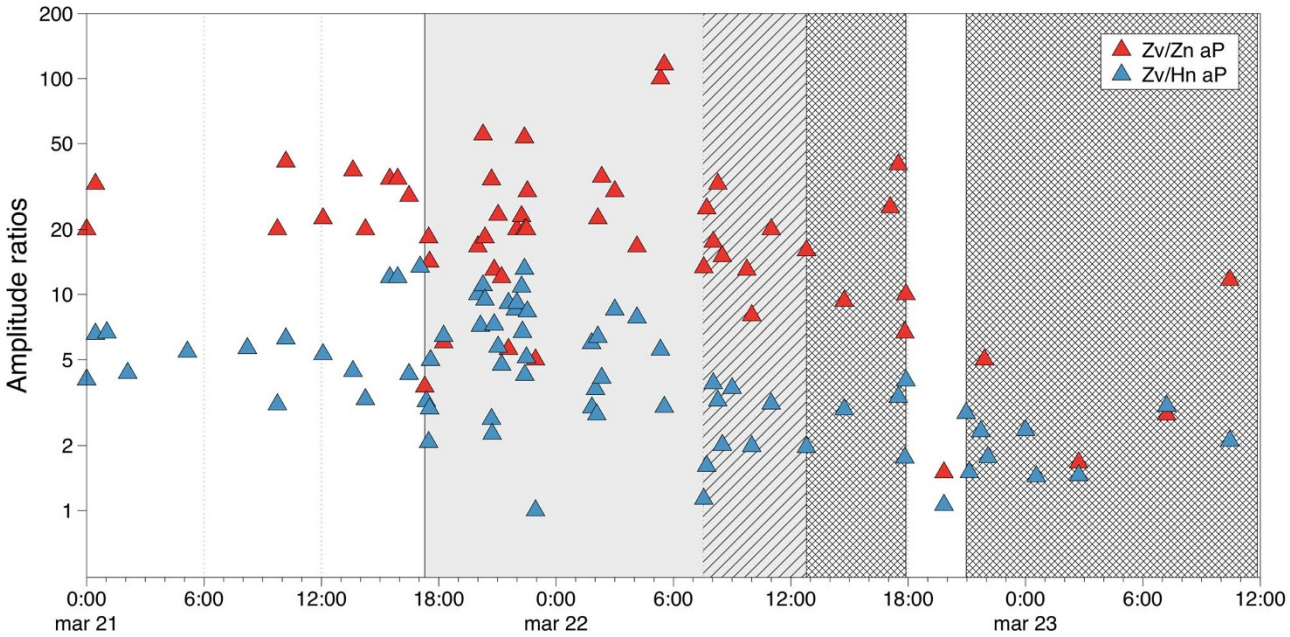

Figure 3 | Amplitude ratios between the prevalent amplitudes of the O.A.M. seismometer at V.O. and the Wiechert seismometer at Naples. Red triangles indicate the ratio between the vertical component of O.A.M. and the vertical component of the Wiechert seismometer. Conversely, blue triangles indicate the ratio between the vertical component of O.A.M. and the horizontal component of the Wiechert seismometer (see text for details).

ning of the lava-fountains (phase II) up to few hours during the most violent paroxysm (phase III). This scenario is in agreement with seismological data showing an increase in the amplitude of tremor signals in correspondence of lava fountains, related to an increased gas ejection rate. This relationship between volcanic tremor amplitude and lava fountains has been observed on various volcanoes, as Kilauea[25] and Etna[26]. Remarkably, changes in both petrological and seismic indicators have preceded the most violent paroxysm of the phase III, with the emission of low crystalline rocks characterized by high number density (32000–40000) tiny (15-10 μm) microlites, associated to variations in the amplitude ratios of seismic signals reflecting a variations in depth and nature of the seismicity.

We consider that these changes are due to the partial collapse of the deeper parts of the plumbing system (figure 7) as testified also by the high abundance of lithic fragments (including also skarn, clinopyroxenites, dunites[32,33]) observed in the corresponding volcanic deposits. This process caused a pressure drop at the top of the underlying chamber and then the fast extrusion of a larger volume of magma (0.2 km^3) in a short time, with a mass eruption rate that shifted from 2.8×10^6 up to 9.7×10^7 kg/s.

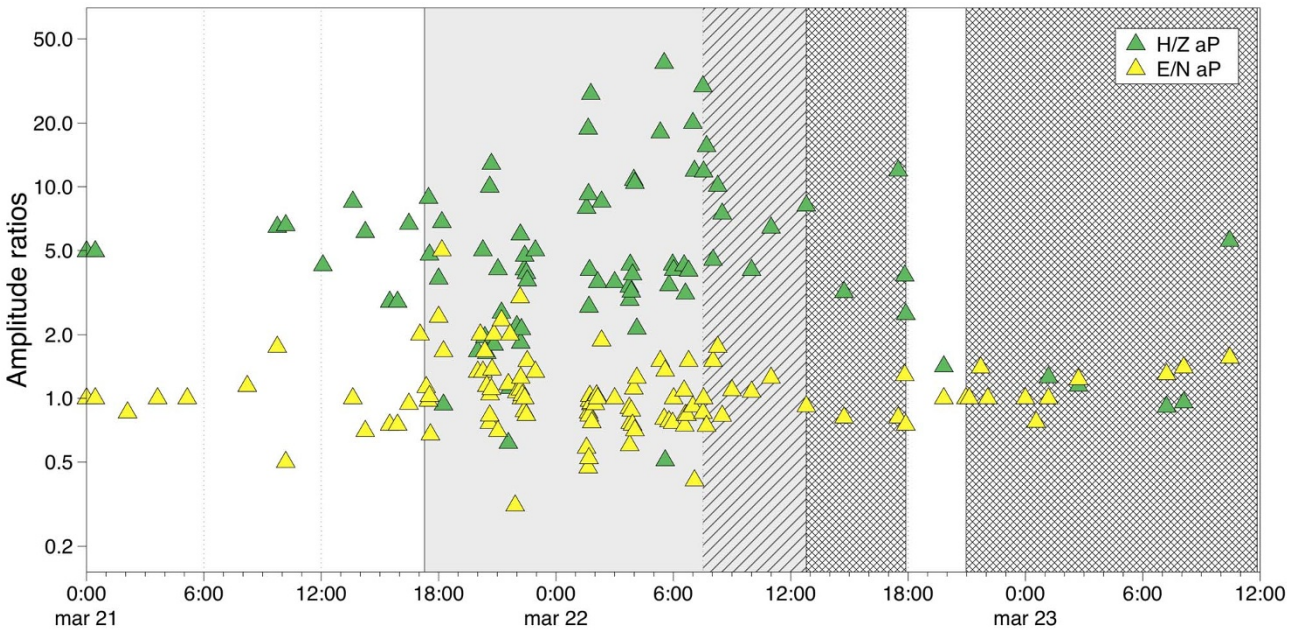

Figure 4 | Amplitude ratios between the horizontal and vertical component of the Wiechert seismometer. Green triangles indicate the ratio between the horizontal and the vertical component, while yellow triangles indicate the ratio between the E-W and the N-S components.

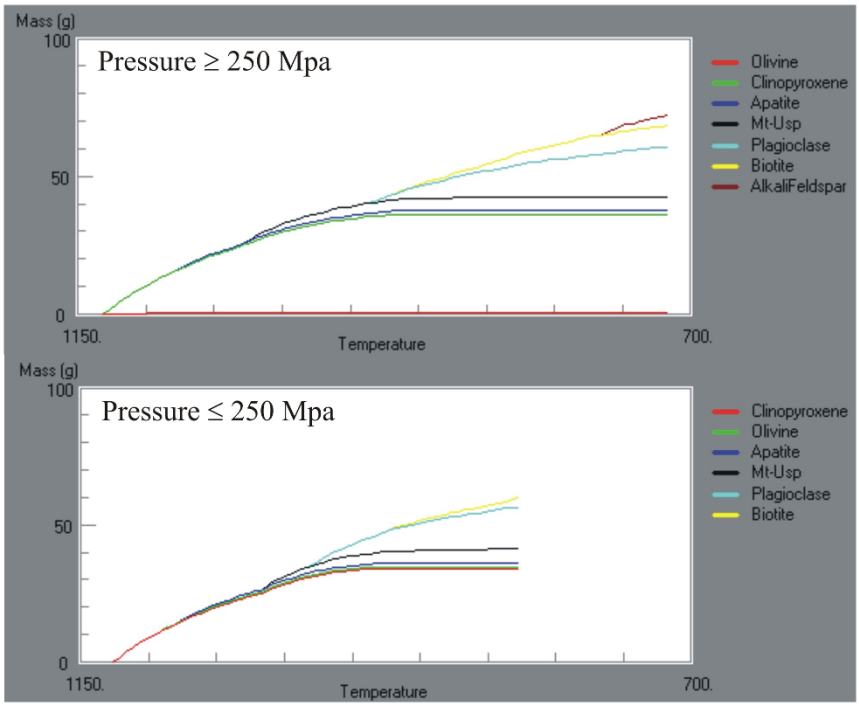

Figure 5 | Mineralogical assemblage during magma cooling in the reservoir as calculated by Melts and Pele program at different P conditions.

The subsequent decrement in magma supply (2.7×10^4 kg/s), as well as the progressive obstruction of the conduit by wall collapse, defines the passage at the final vulcanian phase IV. During the end of the eruption it was observed the emission of large amount of free crystals of leucite and pyroxene that could represent the crystal-mush formed along the wall of the chamber/conduit system and transported on surface by the last remaining liquid.

In conclusion our merged petrological and seismic evidences imply that a complex conduit dynamic, rather than different pre-eruptive condition, was the main cause of the evolution of 1944 eruption of Vesuvius towards violent explosive behavior. Particularly, we documented that the increment of the explosive character of the eruption that culminated in the paroxysmal phase III, was due to the progressive collapse of the deeper part of the conduit that was revealed, since its onset (at the end of the lava-fountains phase II), by robust changes of the petrological and seismic indicators. The reduction of crystallinity and sizes of the microlite and the steepening of the CSD slope during the last part of the phase II, indicate clearly an increase in the ascent rate that cannot be univocally explained by using petrological data alone. However, the contemporaneous change in the seismic amplitude ratios, that reflects the increased contribution of a deeper seismic source, suggests that the incipient collapse of the deeper part of the conduit was the cause of the observed variations in both petrological and seismic indicators. Hence, the joint interpretation of these two independent datasets, points out that an early detection of ongoing modifications within the plumbing system, leading to a sub-plinian phase, can be successfully forecasted at least few hours before the onset of the main explosive phase.

For this reason, we suggest that the development of monitoring methods to evaluate in near-real time petrological features of ejected juvenile material, by using new fast analytical methods[46], during volcanic crisis and their interpretation alongside conventional geophysical monitoring techniques could allow the prompt reconstruction of the ongoing dynamic of the plumbing system and then could be useful for forecasting the eruption evolution (such as the onset of more violent phases).

This is even more important as our groundmass textural data indicate that during the paroxysm, mafic magmas were transferred directly from the deep-seated magma reservoir to the surface at high decompression rate, while residence in upper chambers was limited at the earlier magmatic intrusion. This scenario excludes a long-lasting shallow storage of magma, as suggested elsewhere for strato-volcanos[47], that could act as brake to retard the rapid extrusion of new ascending deeper batches, thus strengthening the chance of hazardous eruptions in the future.

Methods

The volcanic samples were examined under polarized light microscope, scanning electron microscope (JEOL JSM-6500F) and electron microprobe (JEOL-JXA-8200) for textural analysis (microlite shape, number density and size distributions) and the measurements of major and volatile elements (Cl, F, S) concentration in the groundmass glass and in the mineralogical phases. The measurements were carried out at the laboratories of the Istituto Nazionale di Geofisica e Vulcanologia, (Roma).

Textural analysis. Textural analyses of microlite shape, number density and size distribution were carried out on polished thin sections of epoxy-impregnated grains using a standard polarized light microscope for preliminary rock characterization followed by a Field Emission Scanning Electron Microscope (FE-SEM) JEOL JSM-6500F (Istituto Nazionale di Geofisica e Vulcanologia, Roma, Italy) for quantitative measurements. Backscattered electron (BSE) images were processed using Adobe Photoshop and ImageJ software to measure the number, size, and area of microlites. Stereological methods have been used to convert the parameters obtained by studying two-dimensional sections into three- dimensional textural values. Specifically, crystal number densities and size distributions have been obtained with the CSD Corrections 1.3 program[48] that includes corrections for both intersection probability and cut section effects. An estimation of the rock fabric and crystal aspect ratio are necessary for generate accurate CSD data. In the studied samples the rock fabric was massive and the crystal aspect ratio has been calculated with CSDslice program[49]. Results are reported in Table 1.

Geochemical analysis. Analyses of major and volatile elements in groundmass glasses and mineral phases were performed on polished thin sections of epoxy-impregnated grains with a JEOL-JXA-8200 electron microprobe (WD/ED combined micro analyzer). Element concentrations were measured at15 keV, a beam current of 4 nA and a counting time of 10 s on peak and 5 sec on both background. For each analysis, a defocused beam was used to minimize losses of alkalis and volatiles, which were counted first to avoid diffusion effects. We attempted to obtain at least ten analyses for each sample. Data reduction was carried out using the ZAF software. The analytical uncertainty was about 1% for most elements.

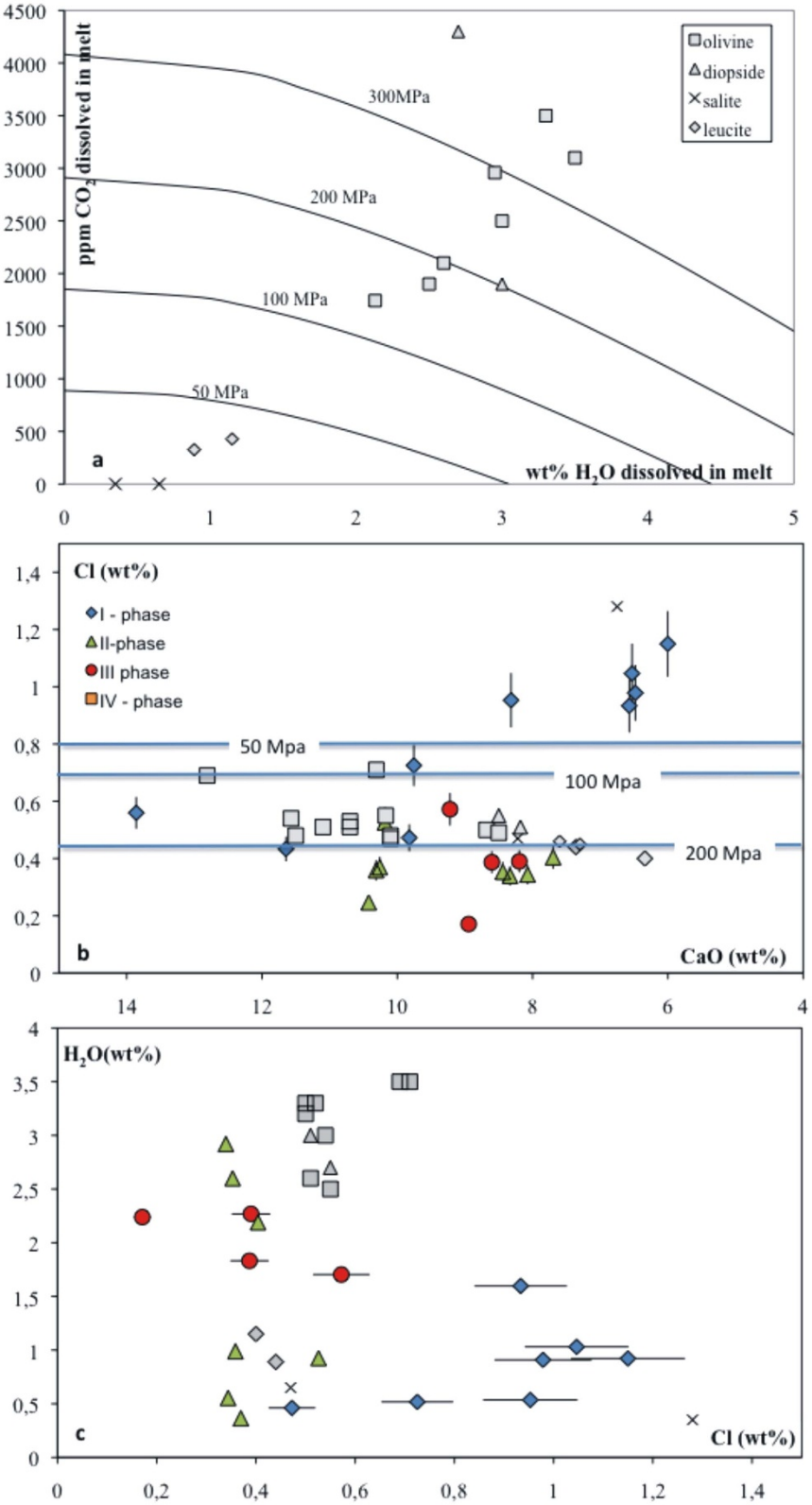

Figure 6 | Behavior of volatile in groundmass glasses (this work, colored symbols) and melt inclusions[30–32] (data from literature, grey symbols). a) Isobars (100 to 400 MPa) for H_2O and CO_2 calculated on the basis of VolatileCalc Newman and Lowenstern[50]. b) Cl content versus CaO (after Pappalardo and Mastrolorenzo[51]) and c) Cl content versus H_2O. Solubility lines calculated from Signorelli & Carroll[34]. During initial slow ascent, the composition of magma emitted during the effusive phase I follows solubility model both for Cl and water, thus indicating equilibrium degassing during slow ascent in the conduit. On the contrary, the composition of glass samples of explosive phases departs from equilibrium concentrations due to fast ascent preventing fluid/liquid exchange (disequilibrium degassing).

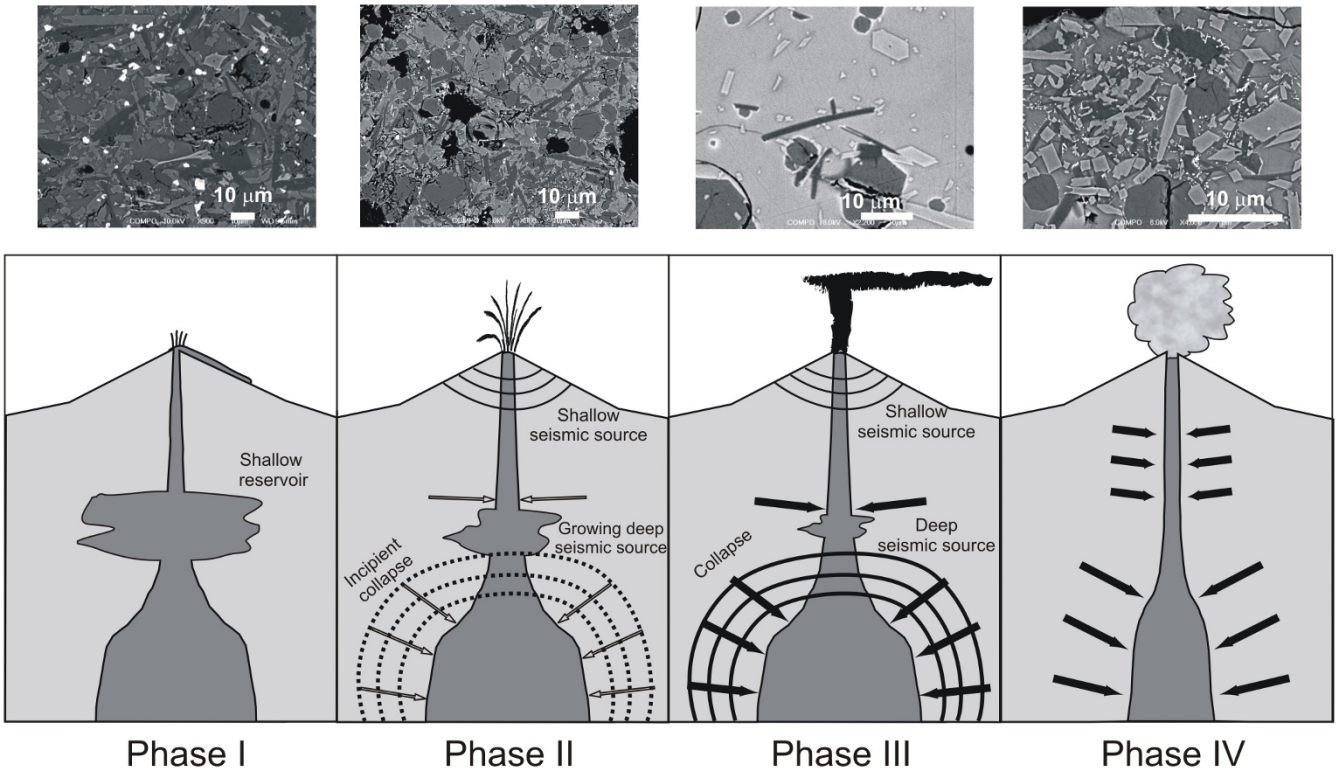

Figure 7 | Schematic diagram for conduit processes and eruption phenomena during the recognized four phases of the Vesuvius 1944 eruption, deduced from the evolution of petrological and seismic indicators. On the top we show examples of textural features representative of products of each eruptive phase. Groundmass texture shows high crystallinity associated to larger prismatic microlites during the first phases of the eruption, while shifts toward low values of crystallinity and size of microlites that became progressively also more skeletal. Phase I (18-21 March) initiated with magma intrusion and stagnation at shallow level during conduit enlargement, the effusive activity lasted about 4 days with a mass discharge rate of 1.4×10^5 kg/s. During phase II (21-22 March) magma experienced an increment in ascent rate due to sudden conduit-vent opening, causing the shift from the effusive to the lava fountains activity, with a mass discharge rate of 2.8×10^6 kg/s. During the phase III (22–23 March) the partial collapse of the deeper parts of the plumbing system caused a pressure drop at the top of the underlying chamber and then the fast extrusion of a larger volume of magma (0.2 km^3) in a short time, with a mass eruption rate up to 9.7×10^7 kg/s. The end of the eruption with the passage at the vulcanian phase IV (24–29 March) is due to both the decrement in magma supply (2.7×10^4 kg/s), as well as to the progressive obstruction of the conduit by wall collapse.

The H_2O content of all analyzed glass was estimated by using the "volatile by difference" method based on EMPA analyses. Results are reported in (supplementary Tables S2 and S3).

1. BBC News, Indonesia volcano Sinabung in deadly eruption". http://www.bbc.com/news/uk-26000359, (2014) Date of Access: 01/02/2014.
2. Houghton, B. F. & Gonnermann, H. M. Basaltic explosive volcanism: constraints from deposits and models. *Chemie der Erde-Geochem.* **68**, 117–140 (2008).
3. D'Auria, L., Giudicepietro, F., Martini, M. & Peluso, R. Seismological insight into the kinematics of the 5 April 2003 vulcanian explosion at Stromboli volcano (southern Italy). *Geophys. Res. Lett.* **33** (2006).
4. Rosi, M. *et al.* A case history of paroxysmal explosion at Stromboli: timing and dynamics of the April 5, 2003 event. *Earth Planet. Sci. Lett.* **243**, 594–606 (2006).
5. Métrich, N., Bertagnini, A., Landi, P., Rosi, M. & Belhadj, O. Triggering mechanism at the origin of paroxysms at Stromboli (Aeolian Archipelago, Italy): the 5 April 2003 eruption. *Geophys. Res. Lett.* **32** (2005).
6. Bertagnini, A., Di Roberto, A. & Pompilio, M. Paroxysmal activity at Stromboli: lessons from the past. *Bull. Volcanol.* **73**, 1229–1243 (2011).
7. Andronico, D. *et al.* The 15 March 2007 paroxysm of Stromboli: video-image analysis, and textural and compositional features of the erupted deposit. *Bull. Volcanol.* **75**, 1–19 (2013).
8. Hammer, J. E., Cashman, K. V., Hoblitt, R. P. & Newman, S. Degassing and microlite crystallization during pre-climactic events of the 1991 eruption of Mt. Pinatubo, Philippines. *Bull. Volcanol.* **60**, 355–380 (1999).
9. Cashman, K. V. & McConnell, S. M. Multiple levels of magma storage during the 1980 summer eruptions of Mount St. Helens, WA. *Bull. Volcanol.* **68**, 57–75 (2005).
10. Preece, K., Barclay, J., Gertisser, R. & Herd, R. A. Textural and micro-petrological variations in the eruptive products of the 2006 dome-forming eruption of Merapi volcano, Indonesia: Implications for sub-surface processes. *J. Volcanol. Geotherm. Res.* **261**, 98–120 (2013).
11. Imbò, G. *L'Attività Eruttiva Vesuviana e Relative Osservazioni nel Corso dell'Intervallo Eruttivo 1906-1944 ed in Particolare del Parossismo del marzo 1944* (Annali dell'Osservatorio Vesuviano, Naples, 1949).
12. Cole, P. D. & Scarpati, C. The 1944 eruption of Vesuvius, Italy: combining contemporary accounts and field studies for a new volcanological reconstruction. *Geolog. Mag.* **147**, 391–415 (2010).
13. Cubellis, E., Marturano, A. & Pappalardo, L. Le ceneri distali dell'eruzione del Vesuvio del marzo 1944 raccolte a Devoli (Albania). *Quaderni di Geofisica*, **113**, 1–37 (2013).
14. Cubellis, E., Marturano, A. & Pappalardo, L. *L'Eruzione del Vesuvio del Marzo 1944: Testimonianze e Lettura Scientifica dell'Evento (L*'Ambiente Antropico, vol III, 2014).
15. Martì, J. *et al.* Correlation of magma evolution and geophysical monitoring at El Hierro (Canary Islands) 2011–2012 submarine eruption. *J. Petrol.* (2013) doi:10.1093/petrology/egt014.
16. Marsh, B. D. Crystal size distribution (CSD) in rocks and the kinetics and dynamics of crystallization I. Theory. *Contrib. Mineral. Petrol.* **99**, 277–291 (1988).
17. Marsh, B. D. On the interpretation of crystal size distributions in magmatic systems. *J. Petrol.* **39**, 553–599 (1998).
18. Cashman, K. & Marsh, B. Crystal size distribution (CSD) in rocks and the kinetics and dynamics of crystallization II: Makaopuhi lava lake. *Contrib. Mineral. Petrol.* **99**, 292–305 (1988).
19. Higgins, M. D. Verification of ideal semi-logarithmic, lognor- mal or fractal crystal size distributions from 2D datasets. *J. Volcanol. Geotherm. Res.* **154**, 8–16 (2006).
20. Jerram, D. A., Cheadle, M. J. & Philpotts, A. R. Quantifying the building blocks of igneous rocks: are clustered crystal frame- works the foundation? *J. Petrol.* **44**, 2033–2051 (2003).
21. Turner, S., George, R., Jerram, D. A., Carpenter, N. & Hawkesworth, C. Case studies of plagioclase growth and residence times in island arc lavas from Tonga and the Lesser Antilles, and a model to reconcile discordant age information. *Earth Planet. Sci. Lett.* **214**, 279–294 (2003).

22. Boorman, S., Boudreau, A. & Kruger, F. J. The Lower Zone Critical-Zone transition of the Bushveld Complex: a quantitative textural study. *J. Petrol.* **45**, 1209–1235 (2004).
23. Giudicepietro, F. *et al*. Seismological monitoring of Mount Vesuvius (Italy): more than a century of observations. *Seismol. Res. Lett.* **81**, 625–634 (2010).
24. Imbò, G. *Sismicità Del Parossismo Vesuviano del Marzo 1944* (Annali Osservatorio Vesuviano, Naples, 1952).
25. Head, J. W. & Wilson, L. Lava fountain heights at Pu'u'O'o, Kilauea, Hawaii: Indicators of amount and variations of exsolved magma volatiles. *J. Geophys. Res.: Solid Earth* **92**, 13715–13719 (1987).
26. Alparone, S., Andronico, D., Lodato, L. & Sgroi, T. Relationship between tremor and volcanic activity during the Southeast Crater eruption on Mount Etna in early 2000. *J. Geophys. Res.: Solid Earth* **108** (2003).
27. Ghiorso, M. S. & Sack, R. O. Chemical mass transfer in magmatic processes. IV. A revised and internally consistent thermodynamic model for the interpolation and extrapolation of liquid-solid equilibria in magmatic systems at elevated temperatures and pressures. *Contrib. Mineral. Petrol.* **119**, 197–212 (1995).
28. Asimow, P. D. & Ghiorso, M. S. Algorithmic Modifications Extending MELTS to Calculate Subsolidus Phase Relations. *Am. Mineral.* **83**, 1127–1131 (1998).
29. Boudreau, A. E. PELE - A version of the MELTS software program for the PC platform. *Comp. Geosci.* **25**, 21–203 (1999).
30. Pappalardo, L. & Mastrolorenzo, G. Short residence times for alkaline Vesuvius magmas in a multi-depth supply system: Evidence from geochemical and textural studies. *Earth Planet. Sci. Lett.* **296**, 133–143 (2010).
31. Marianelli, P., Metrich, N. & Sbrana, A. Shallow and deep reservoirs involved in magma supply of the 1944 eruption ofVesuvius. *Bull. Volcanol.* **61**, 48–63 (1999).
32. Fulignati, P., Marianelli, P., Métrich, N., Santacroce, R. & Sbrana, A. Towards a reconstruction of the magmatic feeding system of the 1944 eruption of Mt Vesuvius. *J. Volcanol. Geotherm. Res.* **133**, 13–22 (2004).
33. Fulignati, P., Marianelli, P. & Sbrana, A. Glass-bearing felsic nodules from the crystallizing sidewalls of the 1944 Vesuvius magma chamber. *Mineral. Mag.* **64**, 263–278 (2000).
34. Shea, T. *et al*. Leucite crystals: surviving witnesses of magmatic processes preceding the 79AD eruption at Vesuvius, Italy. *Earth Planet. Sci. Lett.* **281**, 88–98 (2009).
35. Signorelli, S. & Carroll, M. R. Solubility and fluid-melt partitioning of Cl in hydrous phonolitic melts. *Geochim. Cosmochim. Acta* **64**, 2851–2862 (2000).
36. Rutherford, M. J. & Hill, P. M. Magma ascent rates from amphibole breakdown: experiments and the 1980-1986 Mount St. Helens eruptions. *J. Geophys. Res.* **98**, 19667–19685 (1993).
37. Geschwind, C. H. & Rutherford, M. J. Crystallization of microlites during magma ascent: the fluid mechanics of 1980-1986 eruptions at Mount St Helens. *Bull. Volcanol.* **57**, 356–370 (1995).
38. Hammer, J. E. & Rutherford, M. J. An experimental study of the kinetics of decompression-induced crystallization in silicic melts. *J. Geophys. Res.* **197**, 1–23 (2002).
39. Couch, S., Sparks, R. S. J. & Carroll, M. R. The kinetics of degassing-induced crystallization at Soufrie' re Hills Volcano, Montserrat. *J. Petrol.* **44**, 1477–1502 (2003).
40. Martel, C. & Schmidt, B. C. Decompression experiments as an insight into ascent rates of silicic magmas. *Contribut. Mineral. Petrol.* **144**, 397–415 (2003).
41. Browne, B. L. & Gardner, J. E. The influence of magma ascent path on the texture, mineralogy, and formation of hornblende reac-tion rims. *Earth Planet. Sci. Lett.* **246**, 161–176 (2006).
42. Brugger, C. R. & Hammer, J. E. Crystal size distribution analysis of plagioclase in experimentally decompressed hydrous rhyodacite magma. *Earth Planet. Sci. Lett.* **300**, 246–254 (2010).
43. Armienti, P. *et al*. The long-standing 1991–1993 Mount Etna eruption: petrography and geochemistry of lavas. *Acta Vulcanol.* **4**, 15–28 (1994).
44. Armienti, P., Tonarini, S., Innocenti, F. & D'Orazio, M. Mount Etna pyroxene as tracer of petrogenetic processes and dynamics of the feeding system. In: Beccaluva L, Bianchini G, Wilson M, editors. Cenozoic Volcanism in the Mediterranean Area. *Geol. Soc. Am.* **418**, 265–276 (2007).
45. Orlando, A., D'Orazio, M., Armienti, P. & Borrini, D. Experimental determination of plagioclase and clinopyroxene crystal growth rates in an anhydrous trachybasalt from Mt Etna (Italy). *Europ. J. Mineral.* **20**, 653–664 (2008).
46. Pankhurst, M. J. *et al*. Monitoring the Magmas Fuelling Volcanic Eruptions in Near-real-time Using X-ray Micro-2014, computed Tomography. *J. Petrol.* **55**, 671–684 (2014).
47. Costa, F., Andreastuti, S., Bouvet de Maisonneuve, C. & Pallister, J. S. Petrological insights into the storage conditions, and magmatic processes that yielded the centennial 2010 Merapi explosive eruption. *J. Volcanol. Geotherm. Res.* **261**, 209–235 (2013).
48. Higgins, M. D. Measurement of crystal size distributions. *Am. Mineral.* **85**, 1105–1116 (2000).
49. Morgan, D. J. & Jerram, D. A. On estimating crystal shape for crystal size distribution analysis. *J. Volcanol. Geotherm. Res.* **154**, 1–7 (2006).
50. Newman, S. & Lowenstern, J. B. VolatileCalc: a silicate melt-H_2O-CO_2 solution model written in Visual Basic for Excel. *Comput. Geosci.* **28**, 597–604 (2002).
51. Pappalardo, L. & Mastrolorenzo, G. Rapid differentiation in a sill-like magma reservoir: a case study from the campi flegrei caldera. *Sci. Rep.* **2**, Article number, 712 (2012).

Author contributions

L.P. designed the research, L.P. and L.D. performed the research, analyzed data and wrote the paper, A.C. carried out the electron microprobe analysis, S.F. revised the data from G. Imbò (1952).

Additional information

Supplementary information accompanies this paper at http://www.nature.com/scientificreports

Competing financial interests: The authors declare no competing financial interests.

How to cite this article: Pappalardo, L., D'Auria, L., Cavallo, A. & Fiore, S. Petrological and seismic precursors of the paroxysmal phase of the last Vesuvius eruption on March 1944. *Sci. Rep.* **4**, 6297; DOI:10.1038/srep06297 (2014).